Low-complexity Adaptive Channel Estimation

Xianyu Chen[1] and Ming Jiang[12*]
[1]Sun Yat-sen University, Guangzhou, China
[2]SYSU Shunde Research Institute, Shunde, China
*E-mail: jiangm7@mail.sysu.edu.cn

***Abstract*— Among the numerous channel estimation (CE) techniques in the literature, pilot-aided channel estimation (PACE) has been widely employed, with the aid of various interpolation methods for reducing pilot overhead. Conventional linear interpolation (LI), polar linear interpolation (PLI) and adaptive polar linear interpolation (APLI) methods are easy to implement, but naturally result in residual interpolation errors at high signal-to-noise ratios (SNR). In this paper, we propose an effective origin optimisation aided APLI CE (EOO-APLI-CE) method, which outperforms existing schemes of similar complexity, through both inheriting the benefits offered by conventional APLI and further reducing the residual error floors. Moreover, the proposed real-time EOO-APLI-CE scheme can adapt to any channel model, without the need of channel-model-specific optimisation required, for example, by the conventional APLI method. Last but not least, it maintains a complexity as low as the traditional LI method.**

***Index Terms*— Adaptive polar linear interpolation (APLI), channel estimation (CE), effective origin optimisation (EOO).**

I. Introduction

COHERENT detection has been widely used in existing wireless systems and is also likely in B4G/5G systems [1], for its significant performance gain over noncoherent detection. However, it requires accurate channel information which is usually acquired by the channel estimation (CE) module invoked at the receiver. In the literature, numerous CE methods have been proposed, including pilot-aided CE (PACE) [2], [3], decision-directed CE (DDCE) [4], as well as blind channel estimation (BCE) algorithms [5].

Among the various aforementioned techniques, PACE has shown attractive simplicity, effectiveness and efficiency from implementational perspectives. In PACE-aided systems, interpolation techniques are typically needed, such as linear interpolation (LI), polynomial interpolation (PI) [6], polar linear interpolation (PLI) [7], adaptive polar linear interpolation (APLI) [8], two-dimensional (2D) Wiener filtering [3], [9], Bayesian minimum mean square error channel estimation (BMMSE-CE), least mean square (LMS) filtering [10], etc. Naturally, LI and PLI result in non-negligible residual interpolation errors that exist even under high signal-to-noise ratios (SNR), while 2D Wiener filtering, BMMSE-CE and LMS often suffer from an increased complexity. Moreover, paper [11] proposes some low-complexity channel estimation for cooperative wireless sensor networks, but it does not discuss the corresponding scenario in orthogonal frequency division multiplexing (OFDM) system. Striking a good performance-complexity tradeoff, the recently proposed APLI scheme offers notable improvements upon classical interpolation methods by employing a sliding window (SW), where the so-called effective origin (EO) is calculated and used as a reference point for assisting in the generation of PLI-based channel coefficients between frequency-domain (FD) pilots. However, since the SW in APLI has a fixed length, it may lead to bursty CE errors under highly frequency-selective channels. Furthermore, the SW length has to be separately optimised for different channel models, thus restricting its capability of adapting to real-time scenario switching, for instance when the user equipment (UE) moves from outdoor to indoor channels.

Against this background, we propose an effective origin optimisation aided APLI (EOO-APLI) scheme, which exploits simple geometric calculations to derive a more accurate EO, such that more robust interpolated channel coefficients can be obtained, regardless of the specific channel model and/or real-time channel conditions. Thanks to its capability of adaptively tracking the channel's instantaneous fading variation in any channel models, the proposed EOO-APLI-aided channel estimation (EOO-APLI-CE) scheme operating in the FD outperforms a range of existing schemes, while maintaining a low computational complexity. Furthermore, our proposal is readily applicable to any FD-PACE schemes using interpolations, for example in OFDM systems.

The rest of this paper is organised as follows. In Section II, the APLI-CE scheme is briefly reviewed. Then, the proposed EOO-APLI-CE framework is introduced in Section III, followed by the numerical results in Section IV. Finally, we conclude our findings in Section V.

II. System Procedure

The proposed EOO-APLI-CE scheme is illustrated in Fig. 1, where the newly added modules are printed in gray colour, while the remaining modules are the same as in the conventional APLI-CE of [8].

Assume that N data symbols are inserted between every two of the total P FD pilot symbols in a general OFDM system. At the k^{th} pilot subcarrier, the initial estimated FD channel transfer function (FD-CTF) $\hat{H}_{\mathrm{LS}}[k]$ is obtained for predefined pilot $s_p[k]$ based on the least squares (LS) principle as

$$\hat{H}_{\mathrm{LS}}[k] = \frac{s_p^*[k]}{|s_p[k]|^2}\cdot x[k] = H[k] + \frac{s_p^*[k]}{|s_p[k]|^2}\cdot v[k],\ 0 \le k \le P-1, \tag{1}$$

where $(\cdot)^*$ denotes the conjugate operation, $x[k]$ is the received symbol, and $v[k]$ is the complex additive white Gaussian noise (AWGN) sample with zero mean and unit variance. Then the proposed EOO procedure is invoked to calculate a reference point, c_k, which is referred to as the EO. In the conventional

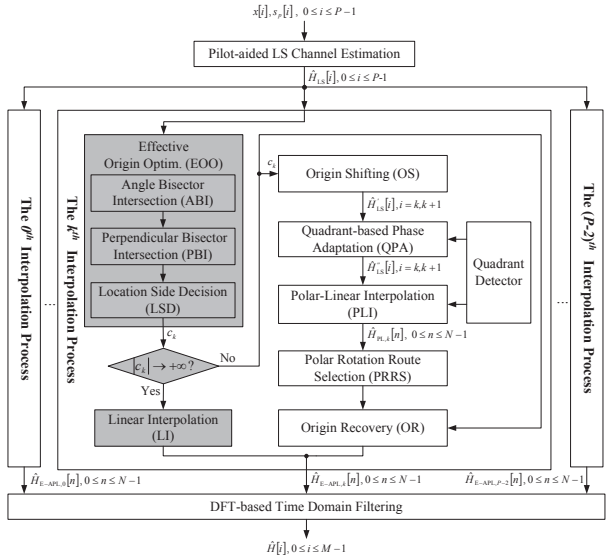

Fig. 1. The flowchart of the proposed EOO-APLI-CE scheme.

APLI-CE scheme, the EO is obtained by taking average over the LS estimates within a predefined SW of fixed length W, as detailed in [8, (7)]. Since different channel models have various characteristics, a channel-dependent value of W has to be determined, which is practically inconvenient due to the large variety of channel models. Furthermore, as the channel conditions in realistic scenarios can vary significantly, for example when the UE moves from outdoor to indoor location, using a predefined fixed-length SW becomes suboptimal. In contrast, our new EOO method is capable of largely improving the accuracy of EO, as to be detailed in Section III, where we will elaborate on the three sub-modules.

In the next step, the origin shifting (OS) [8] procedure will be used to shift the origin of the complex plane to the EO. Then, the quadrant detector decides in which quadrant of the complex plane the origin-shifted effective LS estimates $\hat{H}'_{\rm LS}[\cdot]$ are located. Based on such information, a procedure called quadrant-based phase adaptation (QPA) is employed to revise the phases of the origin-shifted LS estimates based on [8, (9)], resulting in the QPA-calibrated LS estimates denoted by $\hat{H}''_{\rm LS}[\cdot]$. Then, the APLI-CE scheme would generate N polar-linearly interpolated FD-CTFs for the data symbols between the k^{th} and the $(k+1)^{th}$ pilots [7]

$$\hat{H}_{{\rm PL},k}[n] = \hat{A}_{{\rm PL},k}[n] \cdot e^{j\hat{\alpha}_{{\rm PL},k}[n]},\ n = 0, \cdots, N-1, \quad (2)$$

where

$$\begin{cases} \hat{A}_{{\rm PL},k}[n] = \hat{A}''_{\rm LS}[k] + \Delta_A[k] \cdot (n+1) \\ \hat{\alpha}_{{\rm PL},k}[n] = \hat{\alpha}''_{\rm LS}[k] + \Delta_\alpha[k] \cdot (n+1) \end{cases}, \quad (3)$$

and the interpolation steps $\Delta_A[k]$ and $\Delta_\alpha[k]$ are defined by:

$$\begin{cases} \Delta_A[k] = \frac{1}{N+1}(\hat{A}''_{\rm LS}[k+1] - \hat{A}''_{\rm LS}[k]) \\ \Delta_\alpha[k] = \frac{1}{N+1}(\hat{\alpha}''_{\rm LS}[k+1] - \hat{\alpha}''_{\rm LS}[k]) \end{cases}, \quad (4)$$

while $\hat{A}''_{\rm LS}[\cdot]$ and $\hat{\alpha}''_{\rm LS}[\cdot]$ denote the amplitude and the phase of $\hat{H}''_{\rm LS}[\cdot]$, respectively.

Then, exploiting PLI-based estimates $\hat{H}_{{\rm PL},k}[n]$, the polar rotation route selection (PRRS) [8] function shown in Fig. 1 selects the best polar rotation route (PRR), which is defined as the optimised two-dimensional (2D) directional trajectory formed by the set of the aforementioned PLI-generated FD-CTF estimates $\hat{H}''_{\rm LS}[\cdot]$. Those FD-CTF estimates on the best PRR are then considered as the solution. With the aid of EO, they will be shifted back to their original locations corresponding to the initial origin of the complex plane. Finally, discrete Fourier transform (DFT) based time-domain (TD) filtering [2] is employed for reducing interpolation-induced noise, resulting in the output channel estimates $\hat{H}[i],\ 0 \le i \le M-1$, where $M = N \cdot P - N + P$, to be used for FD data symbol detection.

III. The Proposed EOO-APLI-CE Scheme

The EOO module is the key function of the proposed EOO-APLI-CE scheme. It is designed in a way, such that it can be seamlessly integrated with the conventional APLI-CE scheme, while offering a much more accurate real-time tracking capability on the FD-CTFs' instantaneous contour than that of APLI-CE. Furthermore, such benefits are achieved without incurring additional computational complexity. More precisely, EOO steers the local position of the EO to ensure that each and every local portion of the estimated FD-CTF contour smartly fits its true versions, as detailed in the sequel.

More specifically, the proposed EOO algorithm includes three sub-modules, namely the angle bisector intersection (ABI), the perpendicular bisector intersection (PBI) and the location side decision (LSD) operators.

A. The ABI Sub-module

In order to determine the EO for the pilot estimate pair $\hat{H}_{\rm LS}[k]$ and $\hat{H}_{\rm LS}[k+1]$, which are given by (1), four consecutive pilot estimates $\hat{H}_{\rm LS}[l]$, where $l = \{k-1, k, k+1, k+2\}$, are exploited in the ABI procedure.

More specifically, the angle bisector through $\hat{H}_{\rm LS}[k]$ is

$$y = \hat{H}_{\rm LS}[k] + k_1 n_1, \quad (5)$$

where $k_1 \in \mathbb{R}$ and $n_1 = \frac{r_{k,k-1}}{|r_{k,k-1}|} + \frac{r_{k,k+1}}{|r_{k,k+1}|}$ suggests the direction of that specific angle bisector, while $r_{i,j} = \hat{H}_{\rm LS}[j] - \hat{H}_{\rm LS}[i]$ indicates the pseudo-chord vector from point $\hat{H}_{\rm LS}[i]$ to point $\hat{H}_{\rm LS}[j]$. Similarly, the angle bisector through $\hat{H}_{\rm LS}[k+1]$ is

$$y = \hat{H}_{\rm LS}[k+1] - k_2 n_2, \quad (6)$$

where $k_2 \in \mathbb{R}$ and $n_2 = \frac{r_{k+1,k}}{|r_{k+1,k}|} + \frac{r_{k+1,k+2}}{|r_{k+1,k+2}|}$. Then, the intersection point of the two angle bisectors denoted by (5) and (6), namely the optimised version of the EO c_k, can be calculated by

$$c_k = \hat{H}_{\rm LS}[k] + k_1 n_1 = \hat{H}_{\rm LS}[k+1] - k_2 n_2, \quad (7)$$

which can be transformed to

$$k_1 n_1 + k_2 n_2 = r_{k,k+1} = \hat{H}_{\rm LS}[k+1] - \hat{H}_{\rm LS}[k]. \quad (8)$$

Based on (8) and noting $k_1, k_2 \in \mathbb{R}$, we arrive at

$$c_k = \frac{r_{k,k+1} n_2^* - r_{k,k+1}^* n_2}{n_1 n_2^* - n_1^* n_2} n_1 + \hat{H}_{\rm LS}[k]. \quad (9)$$

Then, c_k of (9) can be used as the EO for $\hat{H}_{\rm LS}[k]$ and $\hat{H}_{\rm LS}[k+1]$. Note that if the denominator in (9) satisfies $n_1 n_2^* - n_1^* n_2 = 0$, it implies that $\Im(n_1 n_2^*) = 0$ and (9) leads to $|c_k| \to +\infty$. Let $n_i = |n_i| \cdot e^{j \cdot \angle n_i}$ $(i = \{1, 2\})$, where the operators $|\cdot|$ and $\angle(\cdot)$ denote the amplitude and the phase angle of n_i, respectively. Then it yields $|n_1| \cdot |n_2| \cdot \sin(\angle n_1 - \angle n_2) = 0 \Rightarrow \angle n_1 - \angle n_2 = k\pi$ $(k \in \mathbb{Z})$, which indicates that the direction vectors n_1 and n_2 are mutually parallel. This means that in the ABI sub-module, the two angle bisectors are mutually parallel when the condition of $|c_k| \to +\infty$ is fulfilled. However, this is an impossible event according to Lemma 1, which is proved in Appendix A:

Lemma 1: In the ABI sub-module, the probability of $|c_k| \to +\infty$ is equal to zero.

Therefore, it is guaranteed that the ABI sub-module, if activated, will provide an improved c_k of a finite value, which is more accurate than that offered by conventional APLI.

B. The PBI Sub-module

The PBI sub-module determines an improved EO based on the perpendicular bisector theory. Assume three LS-based FD-CTF estimates, for example $\hat{H}_{\rm LS}[l]$, where $l = \{k-1, k, k+1\}$. Then, the perpendicular bisector of the pseudo-chord connecting $\hat{H}_{\rm LS}[k-1]$ and $\hat{H}_{\rm LS}[k]$ is defined by

$$z = x + k_1 n_1, \tag{10}$$

where $x = \frac{\hat{H}_{\rm LS}[k-1] + \hat{H}_{\rm LS}[k]}{2}$, $k_1 \in \mathbb{R}$ and $n_1 = \xi \cdot \frac{r_{k,k-1}}{|r_{k,k-1}|}$ indicates the direction of perpendicular bisector with $\xi \in \{\sqrt{-1}, -\sqrt{-1}\}$. Similarly, the perpendicular bisector of the pseudo-chord connecting $\hat{H}_{\rm LS}[k]$ and $\hat{H}_{\rm LS}[k+1]$ is

$$z = y - k_2 n_2, \tag{11}$$

where $y = \frac{\hat{H}_{\rm LS}[k] + \hat{H}_{\rm LS}[k+1]}{2}$, $k_2 \in \mathbb{R}$ and $n_2 = \xi \frac{r_{k+1,k}}{|r_{k+1,k}|}$. Then, the intersection point of the two perpendicular bisectors denoted by (10) and (11) can be calculated by

$$c_k = x + k_1 n_1 = y - k_2 n_2, \tag{12}$$

which can be used as an improved EO. Using (12), we obtain

$$k_1 n_1 + k_2 n_2 = y - x. \tag{13}$$

Based on (13) with $k_1, k_2 \in \mathbb{R}$, we can get

$$c_k = \frac{(y-x) n_2^* - (y^* - x^*) n_2}{n_1 n_2^* - n_1^* n_2} n_1 + x. \tag{14}$$

Note that if $n_1 n_2^* - n_1^* n_2 = 0$, then (14) yields $|c_k| \to +\infty$. For the similar reason as discussed in the ABI case, such a condition implies that the two perpendicular bisectors are mutually parallel. Fortunately, it is an event that will not occur in the PBI sub-module. Specifically, we prove the following Lemma 2 in Appendix B:

Lemma 2: In the PBI sub-module, the probability of $|c_k| \to +\infty$ is equal to zero.

Hence, it is also guaranteed that the PBI sub-module, if activated, will provide a c_k that is better than that derived by conventional APLI.

To demonstrate the vital contributions of the proposed EOO algorithm in a clearer manner, we provide some ABI and PBI examples in Fig. 2. As seen in Fig. 2, if we use the method of APLI [8], the position of EO can vary significantly subject to the predefined SW size W. This is expected, since it cannot, in real time, provide a *single* optimum W value to fit *all* instances of the local FD-CTF contours. As a result, such a high variance in EO positions could largely degrade the accuracy of local FD-CTF estimates. In contrast, our proposed EOO method exploits two theoretically-proven submodules, namely ABI and PBI, which are capable of obtaining a much more accurate EO position that tends to be the centre of the round-shape contour constituted by the local FD-CTFs, as illustrated in Fig. 2. Thus, the proposed EOO scheme provides a substantially improved, stable way to catch the local centre of the FD-CTFs' evolvements, regardless of their specific instantaneous variations. This efficiently solves the problem of tracking the local FD-CTF centre in real time, and therefore offers a much more robust performance than the conventional APLI-CE method.

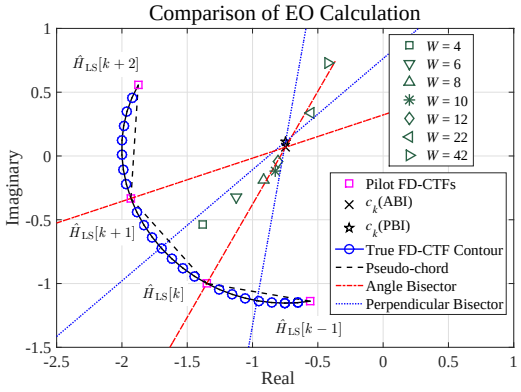

Fig. 2. Comparison of different strategies for EO calculation.

C. The LSD Sub-module

Since FD-CTFs are the DFT of channel impulse response (CIR), the FD-CTF contour is clockwise. This implies that c_k, as the EO, is usually at the right-hand side of the pseudo-chord vector $r_{k,k+1}$. However, in the unlikely event that c_k happens to be at the left-hand side of $r_{k,k+1}$, the ABI and PBI procedures may not work as expected. Furthermore, the c_k value calculated by conventional APLI may also result in a wrong PRR and thus produce a bad performance. Hence, it is necessary to judge at which side c_k is located with respect to $r_{k,k+1}$, which constitutes the task of the LSD sub-module.

More specifically, we define a LSD control factor

$$\beta = \frac{-j \cdot r_{k,k+1}}{c_k - \hat{H}_{\rm LS}[k+1]}, \tag{15}$$

where $-j \cdot r_{k,k+1}$ is a vector perpendicular to $r_{k,k+1}$ with its direction pointing towards the right-hand side of $r_{k,k+1}$. Noting that $\angle\beta$ represents the angle between $-j \cdot r_{k,k+1}$ and $c_k - \hat{H}_{\rm LS}[k+1]$, if the real part of β satisfies $\Re(\beta) > 0$, we can infer that the EO c_k is at the right-hand side of $r_{k,k+1}$.

Finally, we summarise the proposed EOO method in Algorithm 1, where an empirical parameter ρ is introduced to determine the activation of ABI, PBI or APLI procedures.

Furthermore, ω_1 and ω_2 denote the angles obtained by counterclockwise rotating $r_{k-1,k}$ to $r_{k,k+1}$ and $r_{k,k+1}$ to $r_{k+1,k+2}$, respectively.

Algorithm 1 Effective Origin Optimisation (EOO)

1: **Initialisation:** Obtain $\hat{H}_{\rm LS}[l],\ l = k-1, k, k+1, k+2$. Set $\omega_1 = \text{angle}(\frac{r_{k,k+1}}{r_{k-1,k}})$, $\omega_2 = \text{angle}(\frac{r_{k+1,k+2}}{r_{k,k+1}})$. Choose the values of ρ as well as the minimum and maximum SW size $W_{\min}$ and $W_{\max}$, respectively.
2: **if** $0 < |\omega_1| < \rho$ **and** $|\omega_2| \geq \rho$ **then**
3: Calculate (14) by using $\hat{H}_{\rm LS}[l],\ l = k-1, k, k+1$, yielding the PBI-based c_k.
4: **else if** $0 < |\omega_2| < \rho$ **and** $|\omega_1| \geq \rho$ **then**
5: Calculate (14) by using $\hat{H}_{\rm LS}[l],\ l = k, k+1, k+2$, yielding the PBI-based c_k.
6: **end if**
7: **if** PBI-based c_k is available **and** $\Re(\beta) > 0$ in (15), **goto** 15.
8: Calculate (9) by using $\hat{H}_{\rm LS}[l],\ l = k-1, k, k+1, k+2$, yielding the ABI-based c_k.
9: **if** $0 < |\omega_1| < \rho$ **and** $0 < |\omega_2| < \rho$ **or** $\Re(\beta) > 0$ in (15), **goto** 15.
10: **for** $W = W_{\min} : 2 : W_{\max}$ **do**
11: Calculate (7) in [8], yielding the conventional APLI based c_k.
12: **if** $\Re(\beta) > 0$ in (15), **goto** 15.
13: **end for**
14: Set $|c_k| = +\infty$.
15: **Return:** c_k as the EO.

IV. Simulation Results

As an example, the 9-path LTE EVA channel model [12] was used, though other channel models are equally applicable. The Alamouti space-time block code (STBC) [13] was used to combine with an OFDM system of 2048 subcarriers, where a multi-antenna configuration of 2×2 and a 64 quadrature amplitude modulation (64-QAM) were employed. To focus on the evaluation on CE, channel coding was not invoked in this work. Similar to LTE PDSCH transmissions, we used a FD and TD pilot spacing of 6 subcarriers and 7 OFDM symbols, respectively, as a pilot pattern, indicating a very low pilot overhead of 2.38%. As one of the popular configurations supported by LTE [14], pilot symbols were power-boosted by 3 dB in comparison to data symbols. The EOO-APLI-CE scheme is applied in the FD before LI in TD is invoked. Furthermore, we set $W_{\min} = 4$, $W_{\max} = 20$ and $\rho = \frac{\pi}{2}$ in Algorithm 1 based on preliminary simulation tests.

In Fig. 3, the frame error rate (FER) performances of APLI-CE [8] and EOO-APLI-CE are compared, assuming a UE velocity of 30km/h, where one frame is constituted by 14 OFDM symbols, each containing 256 subcarriers, which corresponds to about 20 allocated resource blocks (RB) in LTE systems. As observed from Fig. 3, the choice of W affects the achievable FER of APLI-CE, especially under high E_b/N_0. Thus, in APLI-CE, W has to be optimised offline for different systems under different channel models, since the optimal value of $W = 10$ for the 2×2 STBC-aided system under the EVA channel, as seen in Fig. 3, is not necessarily the optimal value for other cases. In contrast, while largely outperforming APLI-CE in terms of FER, the proposed EOO-APLI-CE scheme eliminates the need of SW and the associated system/channel dependent offline optimisation, thus offering a substantially improved flexibility.

Next, we compare the mean square error (MSE) and FER performances of the different CE schemes in Fig. 4. Besides

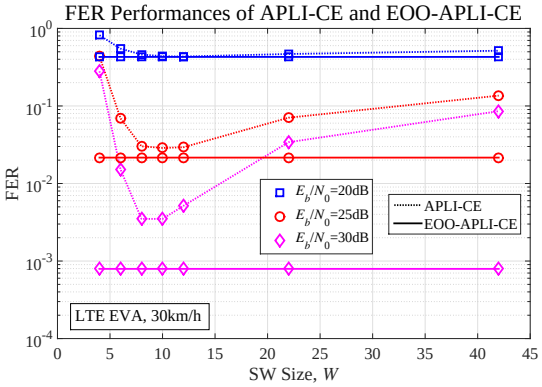

Fig. 3. FER performances of EOO-APLI-CE and APLI-CE.

the ideal CE reference, the LI, PI [6], PLI [7] and APLI [8] schemes are used for fair comparison, which have similar complexities as EOO-APLI-CE. As noted from Fig. 4, the proposed EOO-APLI-CE scheme provides a decent gain in terms of the MSE and FER performances. For example, at a target FER of 10^{-3}, EOO-APLI-CE has only about 2.5dB gap in E_b/N_0 from the ideal CE benchmarker.

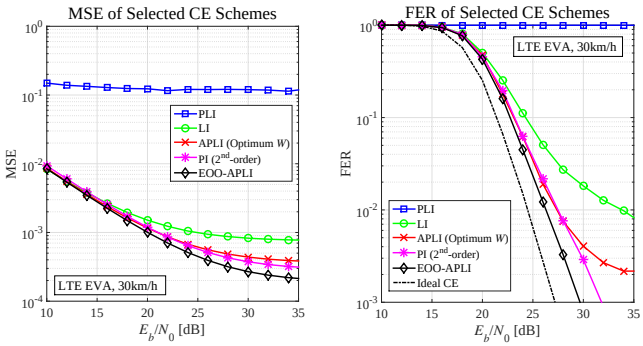

(a) MSE performance. (b) FER performance.

Fig. 4. Performance comparison of various CE schemes.

Furthermore, the computational complexity of the proposed EOO-APLI-CE is similar to that of APLI-CE, with both remaining at the order of LI complexity. This merit is particularly beneficial for power-limited devices. More explicitly, the numbers of complex multiplications in one OFDM symbol for one antenna are $\mathcal{C}^{\rm APLI} = \frac{5}{8}(N+3)P$ [8] and $\mathcal{C}^{\rm EOO-APLI} = \left[\frac{5}{8}N + W_{\max} - W_{\min} + 17\frac{1}{8}\right]P$ for APLI-CE and EOO-APLI-CE, respectively. Note that similar to [8], we have assumed that one complex multiplication is equivalent to four real multiplications in terms of computational complexity.

V. Conclusions

In this paper, we propose an EOO-APLI-CE scheme that invokes the new EOO algorithm, significantly improving the performance of the conventional APLI-CE method. With the aid of simple geometric manipulations, EOO exploits the new submodules of ABI and PBI to obtain a more accurate EO, while ensuring the correct side is selected for FD-CTF contour tracking. Simulation results prove the superiority of the proposed EOO-APLI-CE scheme, which eliminates the

SW required by APLI-CE, and thus increases its flexibility as well as robustness under different channel models.

ACKNOWLEDGEMENT

The funding supports from the General Project of National Natural Science Foundation of China under Grant 61771499, and the Basic Research Project of Guangdong Provincial NSF under Grant 2016A030308008, are gratefully acknowledged.

APPENDIX

A. Proof of Lemma 1

Proof: By the definitions of the two variables ω_i ($i = \{1, 2\}$) used in Algorithm 1 and according to geometry theory, the event $|c_k| \to +\infty$ occurs in the ABI sub-module, iff $\omega_1 + \omega_2 = 2\pi$, as a result of the two angle bisectors being mutually parallel. Considering the stochastic characteristics of the wireless channel and the addition of AWGN at the receiver, both ω_1 and ω_2 are random variables. Since the channel states and AWGN are continuous random variable, the joint probability density function (PDF) of these two random variables, denoted as $f(\omega_1, \omega_2)$, can be considered as a continuous function. Without loss of generality, we assume $0 \leq f(\omega_1, \omega_2) \leq M < +\infty$ for $\forall \omega_1 \in [0, 2\pi)$ and $\forall \omega_2 \in [0, 2\pi)$, where M is a positive number.

Let us now denote the probability of the event $|c_k| \to +\infty$ in the ABI sub-module as

$$P_{\mathrm{ABI}}(|c_k| \to +\infty) = \int_0^{2\pi} \int_{\omega_1 = 2\pi - \omega_2} f(\omega_1, \omega_2) d\omega_1 d\omega_2. \quad (16)$$

Since any probability is non-negative, we have

$$P_{\mathrm{ABI}}(|c_k| \to +\infty) \geq 0. \quad (17)$$

On the other hand, we can derive

$$\begin{aligned} P_{\mathrm{ABI}}(|c_k| \to +\infty) &= \int_0^{2\pi} \int_{\omega_1 = 2\pi - \omega_2} f(\omega_1, \omega_2) d\omega_1 d\omega_2 \\ &\leq \int_0^{2\pi} \int_{\omega_1 = 2\pi - \omega_2} M d\omega_1 d\omega_2 \\ &= \lim_{\triangle^+ \to 0} \int_0^{2\pi} \int_{\omega_1 \geq 2\pi - \omega_2 - \triangle^+}^{\omega_1 \leq 2\pi - \omega_2} M d\omega_1 d\omega_2, \quad (18) \\ &= \lim_{\triangle^+ \to 0} \int_0^{2\pi} \triangle^+ \cdot M d\omega_2 \\ &= 2\pi M \cdot \lim_{\triangle^+ \to 0} \triangle^+ \\ &= 0 \end{aligned}$$

where $\triangle^+$ is a small positive number. Combining (17) and (18), we arrive at $P_{\mathrm{ABI}}(|c_k| \to +\infty) = 0$, which implies that the event $|c_k| \to +\infty$ will not happen in the ABI sub-module. The proof of Lemma 1 completes. ■

B. Proof of Lemma 2

Proof: Note that the event $|c_k| \to +\infty$ occurs in the PBI sub-module, iff $\omega_1 = 0$ or $\omega_1 = \pi$, as a result of the two perpendicular bisectors being mutually parallel. Similar to the ABI case discussed in Appendix A, the PDF of the random variable ω_1, denoted by $g(\omega_1)$, can be considered as a continuous function. Then we assume $0 \leq g(\omega_1) \leq M' < +\infty$ for $\forall \omega_1 \in [0, 2\pi)$, where M' is a positive number.

Let the probability of the event $|c_k| \to +\infty$ be $P_{\mathrm{PBI}}(|c_k| \to +\infty)$. Then we have

$$P_{\mathrm{PBI}}(|c_k| \to +\infty) = \int_{\omega_1 \in \{0, \pi\}} g(\omega_1) d\omega_1 \geq 0. \quad (19)$$

Furthermore, we can derive

$$\begin{aligned} P_{\mathrm{PBI}}(|c_k| \to +\infty) &= \int_{\omega_1 \in \{0, \pi\}} g(\omega_1) d\omega_1 \\ &\leq \int_{\omega_1 \in \{0, \pi\}} M' d\omega_1 \\ &= \lim_{\triangle^+ \to 0} \Big(\int_{\omega_1 \geq 0}^{\omega_1 \leq \triangle^+} M' d\omega_1 + \int_{\omega_1 \geq \pi}^{\omega_1 \leq \pi + \triangle^+} M' d\omega_1 \Big). \\ &= 2M' \cdot \lim_{\triangle^+ \to 0} \triangle^+ \\ &= 0 \end{aligned} \quad (20)$$

Hence, combining (19) and (20), we can obtain $P_{\mathrm{PBI}}(|c_k| \to +\infty) = 0$. Thus, the event $|c_k| \to +\infty$ will not happen in the PBI sub-module. The proof of Lemma 2 completes. ■

REFERENCES

[1] S.-Y. Lien, S.-L. Shieh, Y. Huang, B. Su, Y.-L. Hsu, and H.-Y. Wei, "5G new radio: waveform, frame structure, multiple access, and initial access," *IEEE Communications Magazine*, vol. 55, no. 6, pp. 64–71, Jun. 2017.

[2] M. Jiang, J. Akhtman and L. Hanzo, "Iterative joint channel estimation and multi-user detection for multiple-antenna aided OFDM systems," *IEEE Transactions on Wireless Communications*, vol. 6, no. 8, pp. 2904–2914, Aug. 2007.

[3] F. Pena-Campos, R. Carrasco-Alvarez, O. Longoria-Gandara and R. Parra-Michel, "Estimation of Fast Time-Varying Channels in OFDM Systems Using Two-Dimensional Prolate," *IEEE Transactions on Wireless Communications*, vol. 12, no. 2, pp. 898–907, Feb. 2013.

[4] J. Akhtman and L. Hanzo, "Decision directed channel estimation aided OFDM employing sample-spaced and fractionally-spaced CIR estimators," *IEEE Transactions on Wireless Communications*, vol. 6, no. 4, pp. 1171–1175, Apr. 2007.

[5] C. Shin, R. W. Heath and E. J. Powers, "Blind channel estimation for MIMO-OFDM systems," *IEEE Transactions on Vehicular Technology*, vol. 56, no. 2, pp. 670–685, Mar. 2007.

[6] G. S. Liu and C. H. Wei, "A new variable fractional sample delay filter with nonlinear interpolation," *IEEE Transactions on Circuits and Systems II: Analog and Digital Signal Processing*, vol. 39, no. 2, pp. 123–126, 1992.

[7] R. Weber, "Low-complexity channel estimation for WCDMA random access," in *Proceedings of the 2000 IEEE 52nd Vehicular Technology Conference (VTC '00 Fall)*, vol. 1, 24-28 Sep. 2000, pp. 344–351.

[8] M. Jiang, S. Huang and W. Wen, "Adaptive polar-linear interpolation aided channel estimation for wireless communication systems," *IEEE Transactions on Wireless Communications*, vol. 11, no. 3, pp. 920–926, Mar. 2012.

[9] L. Hanzo, M. Münster and B. J. Choi, *OFDM and MC-CDMA for broadband multi-user communications, WLANs and broadcasting*. Reading, Massachusetts: Wiley, 2004.

[10] G. Liu and L. Zeng and H. Li and L. Xu and Z. Wang, "Adaptive Interpolation for Pilot-Aided Channel Estimator in OFDM System," *IEEE Transactions on Broadcasting*, vol. 60, no. 3, pp. 486–498, Sept. 2014.

[11] P. Ghofrani and T. Wang and A. Schmeink, "A fast converging channel estimation algorithm for wireless sensor networks," *IEEE Transactions on Signal Processing*, vol. 66, no. 12, pp. 3169–3184, June 2018.

[12] 3GPP, "3rd generation partnership project; technical specification group radio access network; spatial channel model for multiple input multiple output (MIMO) simulations (release 10)," TR 25.996 V10.0.0, Mar. 2011.

[13] S. M. Alamouti, "A simple transmit diversity technique for wireless communications," *IEEE Journal on Selected Areas in Communications*, vol. 16, no. 8, pp. 1451–1458, Oct. 1998.

[14] 3GPP, "3rd generation partnership project; technical specification group radio access network; evolved universal terrestrial radio access (E-UTRA); physical layer procedures (release 14)," TS 36.213 V14.4.0, Sept. 2017.